The influence of basal CO_2 on neurofluid dynamics measured using resting-state BOLD fMRI

.

Xiaole Z. Zhong[1,2], Catie Chang[3,4,5] and J. Jean Chen[1,2,6]

1- Rotman Research Institute at Baycrest, Toronto, ON, Canada;
2- Department of Medical Biophysics, University of Toronto, Toronto, ON, Canada;
3-Department of Electrical and Computer Engineering, Vanderbilt University, Nashville, TN, USA;
4-Department of Computer Science, Vanderbilt University, Nashville, TN, USA;
5-Department of Biomedical Engineering, Vanderbilt University, Nashville, TN, USA;
6- Department of Biomedical Engineering, University of Toronto, Toronto, ON, Canada.

Abstract

An understanding of neurofluid dynamics has been gaining importance, in part given the link between neurofluid dynamics and glymphatic flow. As carbon dioxide (CO_2) strongly modulates cerebral blood volume (CBV) and cerebrospinal fluid (CSF) flow, modulation of basal CO2 through different capnic conditions may offer insight into the mechanisms through which neurofluid dynamics are influenced. In this work, we report observations of neurofluid dynamics at normocapnia as well as during short-term hyper- and hypocapnia. We use the resting-state BOLD fMRI signal in neurofluid regions of interest (i.e. blood vessels, CSF compartments) as a surrogate of neurofluid dynamics. From these BOLD signals, we extract the power and central frequency of signal oscillations. We found that 1) Relative to a normocapnic steady state, both hypocapnic and hypercapnic steady states are associated with increased BOLD signal power and shifts in BOLD signal frequency in vascular ROIs in a band-dependent manner; 2) Relative to hypocapnia, hypercapnia is associated with both increased and decreased BOLD signal power in vascular ROIs, depending on the frequency band; 3) these trends are largely reproduced in the CSF ROIs and in the CSF velocity dynamics; 4) these power and frequency variations across capnic conditions are mostly driven by respiratory and heart-rate differences rather than by steady-state CO_2 and associated vascular-tone variations; 5) the cardiac and respiratory response functions differ substantially across capnic conditions. This work contributes to the establishment of the BOLD signal as a surrogate for neurofluid flow, and highlight the role of the autonomic nervous system (ANS) in linking vascular and CSF dynamics in the brain. The findings suggest that the ANS is also instrumental in the regulation of neurofluid flow in response to alterations of cerebral hemodynamic homeostasis. Furthermore, our findings suggest that this mechanism of ANS regulation differs across capnic states, or more broadly, across individuals with different basal capnic states.

Introduction

An understanding of neurofluid dynamics has been gaining importance, in part given the link between neurofluid dynamics and glymphatic flow (Taoka & Naganawa, 2020), which has in turn been linked to dementia pathology (Song et al., 2023). Neurofluids are defined as "fluids in which the central nervous system is immersed, such as blood, cerebrospinal fluid (CSF) and interstitial fluid (ISF)" (Taoka & Naganawa, 2020). Recent studies have highlighted the strong modulatory effects of sleep on CSF flow (Fultz et al., 2019), and in the process cementing the utility of blood-oxygenation-level-dependent (BOLD) resting-state fMRI (rs-fMRI) for monitoring CSF dynamics.

Being sensitive to blood and CSF flow, blood-oxygenation-level-dependent (BOLD) resting-state fMRI (rs-fMRI) has recently enhanced the feasibility of broadening the study neurofluid dynamics (Diorio et al., 2023; Fultz et al., 2019; Yang et al., 2022), although BOLD rs-fMRI's primary application is mapping brain functional connectivity (FC) in health and disease. Past studies have revealed that rs-fMRI functional connectivity patterns are modulated by basal carbon dioxide (CO_2), calling for caution when comparing rs-fMRI data between healthy controls and patients with pulmonary diseases and unusual respiratory patterns such as sleep apnea or chronic obstructive pulmonary disease (Marshall et al., 2015).

Hypercapnia is a commonly used vasodilatory stimulus (Kety & Schmidt, 1948; Reivich, 1964), while hypocapnia may result from artificial ventilation (Lumb, 2017) and in response to hypoxia at high altitudes (Norcliffe et al., 2005). In healthy controls, Biswal et al. showed that FC in the motor cortex was reduced during a hypercapnia baseline (Biswal et al., 1997). The observation was attributed to the CO_2-induced vasodilation that diminished vascular tone and hence the sensitivity of the BOLD signal to hemodynamic fluctuations in rs-fMRI. Indeed, in our previous work, we showed that a hypercapnic baseline (elevated basal end-tidal partial pressure of CO_2 ($PETCO_2$) was associated with sustained or reduced FC in multiple functional networks. As the BOLD signal arises from neurovascular coupling, the reduced FC could arise from reduced vascular tone and reduced neuronal activity during hypercapnia. This reduction in vascular tone results in reduced cerebrovascular reactivity (CVR) (Halani et al., 2015), which in turn modulates cerebrospinal fluid (CSF) dynamics (Wang et al., 2022).

Variations in basal CO_2 are also associated with the frequency of the hemodynamics. Cohen et al., who used hypocapnia and hypercapnia to alter basal CO_2, found that hypercapnia was associated with wider BOLD responses of lower amplitude, while the opposite was true for hypocapnia. The authors concluded that the effect of elevated CO_2 on the vasodilatory mechanisms overcame the effect of increased flow velocity that led to the sluggish hemodynamic response at hypercapnia (E. R. Cohen et al., 2002). Moreover, previous work has shown that slower HRF is associated with higher rs-fMRI spectral power in the low-frequency band (Bailes et al., 2023). Moreover, hypercapnia is known to increase cerebral blood volume (CBV) and CSF volume (van der Kleij et al., 2020). Cerebrovascular and CSF oscillations, two main types of neurofluid dynamics, were recently found to be linked through a temporal derivative (Yang et al., 2022). Thus, there is ample evidence to support hypercapnia and hypocapnia modulating brain hemodynamics.

In this work, we centre our investigation on the result of capnic modulations on neurofluid dynamics as measured using rs-fMRI. We characterize the amplitude (power) and frequency of rs-fMRI fluctuations at different basal $PETCO_2$ levels in regions relevant to neurofluid flow, namely

the macrovasculature and CSF. The macrovasculatar BOLD signal should aggregate blood signals from various networks and thus not be influenced by local changes in neural activity. We hypothesize that: (1) neurofluid fluctuation amplitude variations at different capnic conditions are driven by differences in vascular tone; (2) neurofluid fluctuation frequency variations at different capnic conditions are driven by differences in both vascular tone and respiratory rate (RR) and heart rate (HR). Such a characterization allows us to understand the physiological influence of capnic conditions and how they may influence neurofluid dynamics.

Methods

Data set

This analysis was conducted on 13 participants at hypercapnic, normocapnic and hypocapnic baselines, with further exclusion of two participants due to the absence of physiological measurements, resulting in 11 participants (25-38 years old; 2 males and 9 females) being included in the study. Participants were recruited through the Baycrest Participants Database, consisting of individuals from the Baycrest and local communities. The study was approved by the research ethics board (REB) of Baycrest, and the experiments were performed with the understanding and written consent of each participant, according to REB guidelines.

MRI acquisition

Image acquisition was performed with a Siemens TIM Trio 3 Tesla System (Siemens, Erlangen, Germany), which employed 32-channel phased-array head coil reception and body-coil transmission. rs-fMRI data was acquired using a gradient-echo EPI pulse sequence (TR = 380 ms, TE = 30 ms, FA = 40°, 15 slices, $3.44\times3.44\times5$ mm^3 with 20% slices gap, 950 volumes). T1-weighted MPRAGE anatomical image was acquired (TR = 2400 ms, TE = 2.43 ms, FOV = 256 mm, TI = 1000 ms, readout bandwidth = 180 Hz/px, voxel size = $1\times1\times1$ mm^3). A finger oximeter built into the scanner was used to monitor heart rate, and a pressure-sensitive belt was used to monitor respiration during the rs-fMRI scan.

Gas manipulation

We administered mixtures of O_2, CO_2 and medical air using the RespirAct™ breathing circuit (Thornhill Research, Toronto, Canada) for all gas manipulations. With the sequential gas delivery method (Slessarev et al., 2007), the end-tidal partial pressure of O_2 ($PETO_2$) and CO_2 ($PETCO_2$) pressures can be targeted by computerized and independent means. This setup allowed us to manipulate the basal $PETCO_2$ level of each subject precisely. We separately targeted a normocapnic baseline (subject's nature baseline), a hypercapnic baseline, and a hypocapnic baseline, separated by 4 mmHg CO_2. The RR was self-regulated throughout the respiratory challenges. Hypocapnia is achieved with RespirAct™ primarily through increased breathing depths, and hypercapnia is achieved by increasing CO_2 levels in the air supply. A pseudo-randomized sequence of capnic conditions was used across different subjects, with approximately

two minutes between each condition. During the study, breath-by-breath CO_2 levels were recorded at a rate of 50 Hz using the RespirAct.

Data preprocessing and parameterization

The FreeSurfer reconstruction was performed on the T1 anatomical data for all subjects using FreeSurfer 6.0 (available at: https://surfer.nmr.mgh.harvard.edu). This reconstruction provided tissue segmentation of gray matter, white matter structures, as well as ventricles, which can then be used to delineate regions of interest.

The rs-fMRI data were preprocessed as follows: 1) discard the first 200 volumes, 2) motion correction, 3) motion regression with 6 parameters (3 translations and 3 rotations), 4) demeaning, 5) coregistration with the anatomical image.

Through a frequency-domain group-level independent component analysis (ICA) (Calhoun et al., 2001), we identified three consistent frequency bands across subjects. Specifically, we extracted signals from the neurofluid ROIs of all participants and capnic conditions, and entered them into the ICA. We then identified the frequency spectra corresponding to the three most visually distinct physiologically relevant frequency peaks out of the first 20 independent components. Using these components, we identified frequency bands of interest that are consistent with those reported in previous work (Tong et al., 2019), but are data-driven and specific to the current group of subjects:

(1) Band 1: 0.01-0.14Hz, represents neural activity and vasomotion;
(2) Band 2: 0.14-0.56Hz, reflects respiration;
(3) Band 3: 0.56-1.31Hz. reflects cardiac pulsation.

Based on laser Doppler flowmetry, unstimulated blood flow in Band 1 exhibits 3 spectral peaks. Thus, we divided the BOLD signal in Band 1 into three infraslow bands (Truong et al., 2022), namely:

(1) The endogenic band (Band IS1): 0.001-0.02Hz, represents an endogenic (metabolic) band related to the rhythmic regulation of vascular resistance to the blood flow triggered by variations in blood metabolic substrate concentration (Bracic & Stefanovska, 1998);

(2) The neurogenic band (Band IS2): 0.02-0.04Hz, may result from sympathetic neuronal activity (Kastrup et al., 1989);

(3) The myogenic (Band IS3): 0.06-0.14Hz, which is associated with blood-pressure regulation (Johnson, 1991), and within the range of low-frequency HRV (Akselrod et al., 1981).

Following the formulation in (X. Z. Zhong & Chen, 2022), we further calculated the normalized power (power normalized by signal temporal mean) and the central frequency of each frequency range as follows:

$$\text{frequency at centre of mass} = \frac{\sum_{i=0}^{m} \mathrm{P}_i \mathrm{f}_i}{\sum_{i=0}^{m} \mathrm{P}_i} \quad (1)$$

Where P represents power, and f frequency, and (i = 0,...,m) is the frequency index in the Fourier domain (m corresponds to the maximum frequency).

The resultant frequency maps were then upsampled then segmented into 2 sets of regions of interest (ROIs) using the same method as our previous study (Attarpour et al., 2021): 1) arterial

and venous maps generated directly from rs-fMRI data from the top 20 percentile of signal-fluctuation amplitudes delineated. 2) CSF ROIs were derived either through the use of FreeSurfer tissue segmentation (for the lateral ventricle, third ventricle and fourth ventricle) or by manual delineation (for the cerebral aqueduct).

Moreover, according to previous research, we also calculated a surrogate of CSF velocity by applying the first temporal derivative to the global-mean BOLD signal (GMS) that was detrended and filtered into 0.01-0.1Hz frequency band; for this purpose, we used a zero-delay fourth-order Butterworth filter (Fultz et al., 2019; Yang et al., 2022).

The explanatory variables we tested include: (1) HR; (2) RR; (3) heart rate variability (HRV); (4) respiratory-volume per time (RVT). Both HRV and RVT were estimated based on the method used in the previous study with a window size of 4 seconds (Golestani et al., 2015). As these metrics are relevant to the autonomic nervous system (ANS), and previous work also found a link between global neuronal activity and the ANS, a surrogate of global neural activity, global-mean gray matter signal (GGMS) were also extracted, per definition in (Bolt et al., 2022) (more specifically, averaging time courses of voxels in whole grey matter).

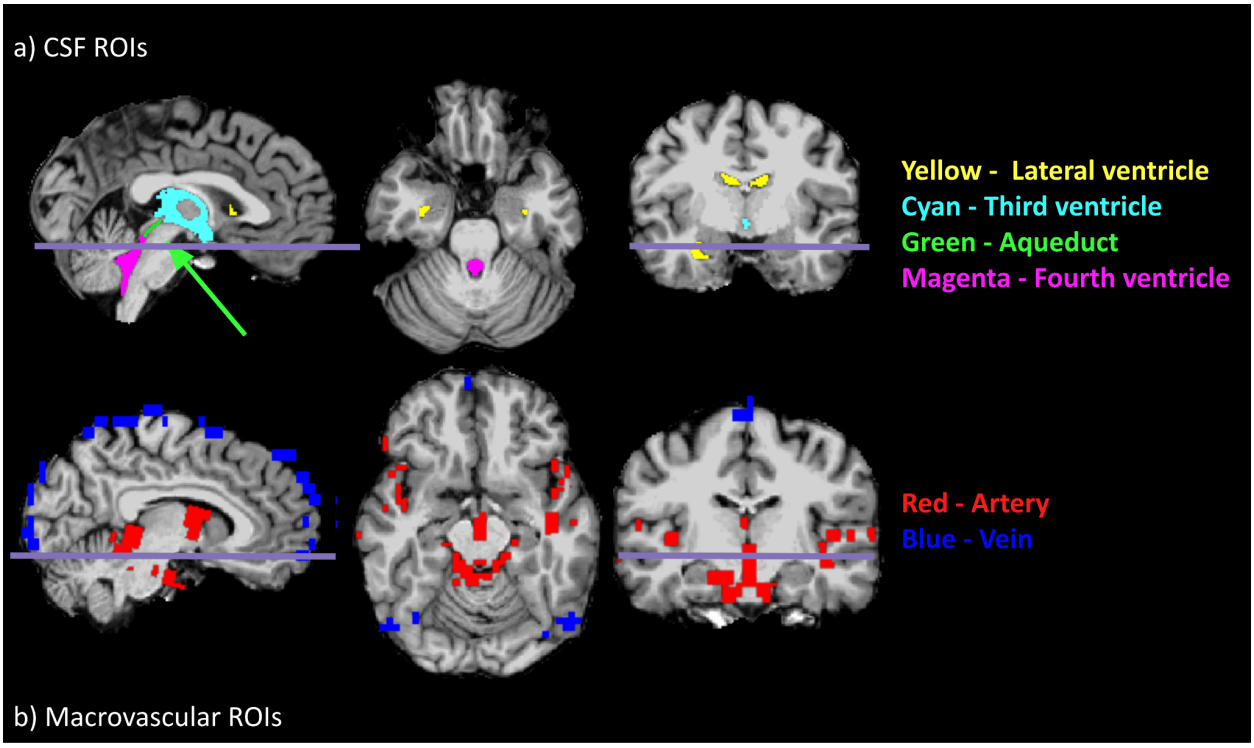

Figure 1. Illustration of the CSF ROI (a) and the vascular ROI (b) from a representative participant. ROIs were colored as described above, the line indicates the position of the transverse slice.

Statistical analysis

Power and central frequency differences across capnic conditions

To demonstrate the difference between power and central frequency for three different capnics, effect sizes were calculated for each band using Glass's estimator (D) for each frequency band (J. Cohen, 1977; Hedges, 1981). The effects were further classified according to the standard set by the previous study (Sawilowsky, 2009) as follows: very small ($D < 0.2$), small ($0.2 < D < 0.5$), medium ($0.5 < D < 0.8$), large ($0.8 < D < 1.2$) and very large ($D > 1.2$).

Association between physiological factors and power and central frequency

An analysis of linear mixed effects was conducted to investigate the association between each physiological factor and the BOLD signal power and central frequency for each frequency band. The input parameters were all demeaned and normalized by its respective inter-subject standard deviation. The variable “ID” was included in the model in order to account for repeated measures within each subject (identified by a subject ID number). Thus, the inter-subject variation is not of interest, as we are modeling the inter-capnic effects as the outcome measure. The model is illustrated in Eq. 2a and 2b. Note that in Band 3, since HRV (Holland & Aboy, 2009) and RVT (Birn et al., 2006) are unlikely to extend into such a high-frequency band, only lower frequency band metrics were incorporated into the linear mixed-effects model (Band 1 for RVT; Bands 1 and 2 for HRV). Band 1 and 2 HRV are taken to represent low-frequency and high-frequency HRV, respectively (Holland & Aboy, 2009). Data sets without coverage of the aqueduct and fourth ventricle were excluded from this analysis.

$$\text{Central Frequency} \sim \text{Intercept} + \text{ID} + \text{Heart Rate} + \text{Respiratory Rate} + \text{PETCO2} + \text{HRV Central Frequrncy} + \text{RVT Central Frequency} \quad (2)$$

$$\text{Power} \sim \text{Intercept} + \text{ID} + \text{Heart Rate} + \text{Respiratory Rate} + \text{PETCO2} + \text{HRV Power} + \text{RVT Power} \quad (3)$$

The 95% confidence interval of each coefficient in the model is determined by bootstrapping (1000 iterations of resampling with replacement), and each coefficient is deemed significant only if its confidence interval does not span zero.

Cardiac and respiratory response function across capnias

To quantify the mediating mechanism of the HRV and RVT on BOLD signal dynamics, the cardiac response function (CRF) and respiratory response function (RRF). For each subject, the mean signal from each neurofluid ROI as well a the GGMS and CSF velocity time series were deconvolved by the corresponding HRV and RVT using the Laguerre expansion (Prokopiou et al., 2018; Shams et al., 2022) for all macrovascular and CSF ROIs as well as GGMS listed above across three capnias.

Interaction between BOLD and respiratory/cardiac variability time series

To quantify the dynamic interaction between BOLD and the ANS parameters HRV and RVT, we calculated the mutual information between these pairs of variables. This permitted us to assess

the interactions unbiased by the accuracies of the response functions. Mutual information was calculated using a MATLAB toolbox (Feed et al. 2015) with the window width (k-nearest-neighbours) chosen to be consistent with the 0.1 Hz bandwidth of the rs-fMRI signal (26 temporal samples). The mutual information index was normalized by the geometric mean. The paired t-test with a threshold of 0.05 was performed to determine whether there were differences between capnias.

Results

Table 1. Physiological measurements (mean and standard deviation). P-values were computed by one-way analysis of variance (ANOVA).

	Hypercapnia	Normocapnia	Hypocapnia	P-value
$PETCO_2$ (mmHg)	42.91±2.47	39.47±1.93	36.44±1.60	1.41e-07
Heart rate (Hz)	1.28±0.32	1.15±0.18	1.26±0.31	0.54
Respiratory rate (Hz)	0.23±0.07	0.23±0.06	0.22±0.06	0.93

In **Table 1**, we illustrated the physiological metrics across the 2 capnic conditions, including $PETCO_2$, heart rate (HR), and respiratory rate (RR). As expected, hypercapnia was associated with the highest $PETCO_2$ levels, followed by normocapnia, with hypocapnia exhibiting the lowest levels. The highest HR was associated with hypercapnia, followed by hypocapnia, with the lowest HR associated with normocapnia. There was an opposite trend in the RR, where normocapnic RR was the highest, followed by hypercapnic and lastly hypocapnic RR. Significant differences across capnic levels were found for $PETCO_2$ but not for the HR and RR in terms of group mean (not equivalent to pairwise differences). Additionally, **Figure 2** shows sample power spectra for vascular and CSF ROIs.

Vascular and CSF oscillations across different capnias

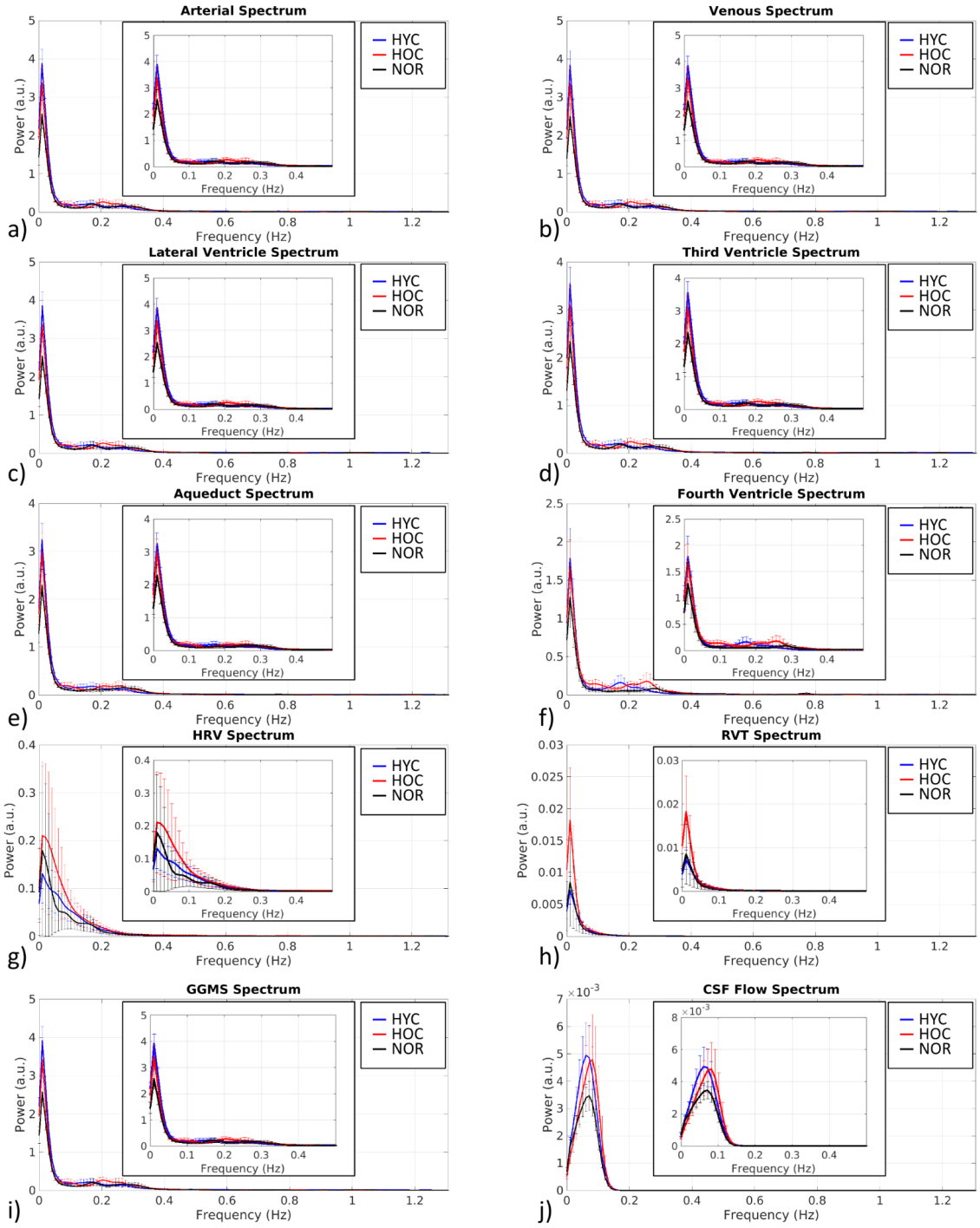

Fig. 2. BOLD signal power spectra in all ROIs. All power values were calculated after time-course normalization by the temporal mean. Spectra were calculated using Welch's method (Hamming window, 41 sample overlaps) and averaged across all participants. The error bars represent ⅓ standard deviation across subjects. The zoomed-in versions of the spectra are shown as insets.

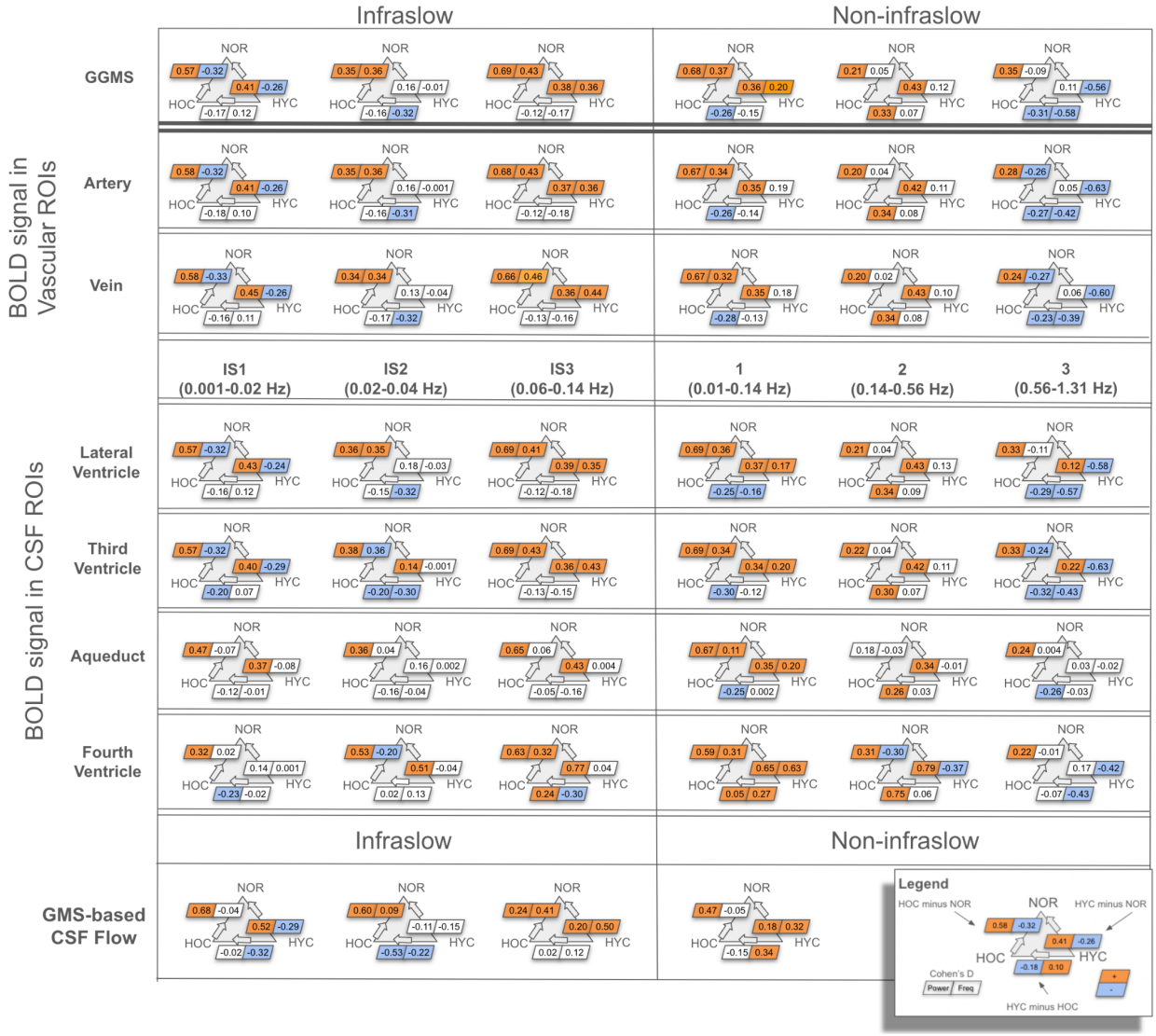

Figure 3. Effect sizes of differences in rs-fMRI oscillation power and frequency across different capnias. NOR: normocapnia; HOC: hypocapnia; HYC: hypercapnia. The figure depicts three infraslow bands (IS1, IS2 and IS3) and three non-infraslow bands (1, 2 and 3) for vascular ROIs (artery and vein), CSF ROIs (lateral ventricle, third ventricle, aqueduct and fourth ventricle) and GMS based CSF flow. We have thresholded the D values in order to present only effects greater than 'small'.

Table 2. An overview of rs-fMRI oscillations across different capnias. Results from neurofluid ROIs and CSF flow are summarized in reference to those from the grey-matter-specific GMS (GGMS). The results were color-coded according to whether BOLD signal power is higher (pink), lower (powder blue), and whether BOLD signal frequency is higher (orange) or lower (blue) in each comparison.

	Hypocapnia, as compared to normocapnia (HOC minus NOR)	**Hypercapnia, as compared to normocapnia (HYC minus NOR)**	**Hypercapnia, as compared to hypocapnia (HYC minus HOC)**
GGMS BOLD	**Higher BOLD signal power in all frequency bands** **Lower BOLD signal frequency in Band IS1 and 3** **Higher BOLD signal frequency in Band IS2, IS3 and 1**	**Higher BOLD signal power in all frequency bands except for Band 3** **Lower BOLD signal frequency in Band IS1 and 3** **Higher BOLD signal frequency in Band IS3**	**Higher BOLD signal power in Band 2** **Lower BOLD signal power in Band IS2, 1 and 3** **Lower BOLD signal frequency in Band IS2 and 3** **Higher BOLD signal frequency in Band 2 (artey only)**
BOLD in vascular ROIs	**Higher BOLD signal power in all frequency bands** **Lower BOLD signal frequency in Band IS1 and 3** **Higher BOLD signal frequency in Band IS2, IS3 and 1**	**Higher BOLD signal power in all frequency bands except for Band 3** **Lower BOLD signal frequency in Band IS1 and 3** **Higher BOLD signal frequency in Band IS3**	**Higher BOLD signal power in Band 2** **Lower BOLD signal power in Band IS2, 1 and 3** **Lower BOLD signal frequency in Band IS2 and 3** **Higher BOLD signal frequency in Band 2 (artey only)**
BOLD in CSF ROIs	**Higher BOLD signal power in all frequency bands** **Lower BOLD signal frequency in Band IS1 and IS2 (3rd and 4th ventricle)** **Higher BOLD signal frequency in Band IS2 (lateral ventricle), IS3 and 1**	**Higher BOLD signal power in all frequency bands (except for Band 3 in the aqueduct and 4th ventricle)** **Lower BOLD signal frequency in Band IS1 and 3** **Higher BOLD signal frequency in Band IS3 and 1 (except for aqueduct and 4th ventricle)**	**Higher BOLD signal power in Band 2** **Lower BOLD signal power in all frequency bands except for Band IS3 and 2** **Lower BOLD signal frequency in Band 1 and 3** **Higher BOLD signal frequency in Band IS2 (3rd ventricle only)**
GMS -based	**Higher CSF-velocity power in all frequency bands**	**Higher CSF-velocity fluctuation power in all frequency bands except for Band IS2**	**Lower BOLD signal power in Band IS2** **Higher CSF-velocity fluctuation frequency in all bands except for Band IS3**

CSF Flow	**Higher CSF-velocity fluctuation frequency in Band IS2 and IS3**	**Lower CSF-velocity fluctuation frequency in Band IS1** **Higher CSF-velocity fluctuation frequency in Band IS2 and 1**	

Signal metrics were compared across capnic conditions, and all associated results are shown as Cohen's D values, as summarized quantitatively in **Fig. 3** as well as verbally in **Table 2**. When comparing hypocapnia to normocapnia, the BOLD signal in vascular and CSF ROIs behaved in very similar ways, and the same is true when comparing hypercapnia to normocapnia. Relative to normocapnia, both hypocapnia and hypercapnia are associated with increased BOLD signal power and shifts in BOLD signal frequency in a band-dependent manner. The behaviour of CSF velocity, only defined for frequencies up to 0.1 Hz, also mimics that of the BOLD signals in the vascular and CSF ROIs. Moreover, GGMS signal metrics behaved very similarly to those from vascular ROIs

Drivers of vascular and CSF oscillations across capnic conditions

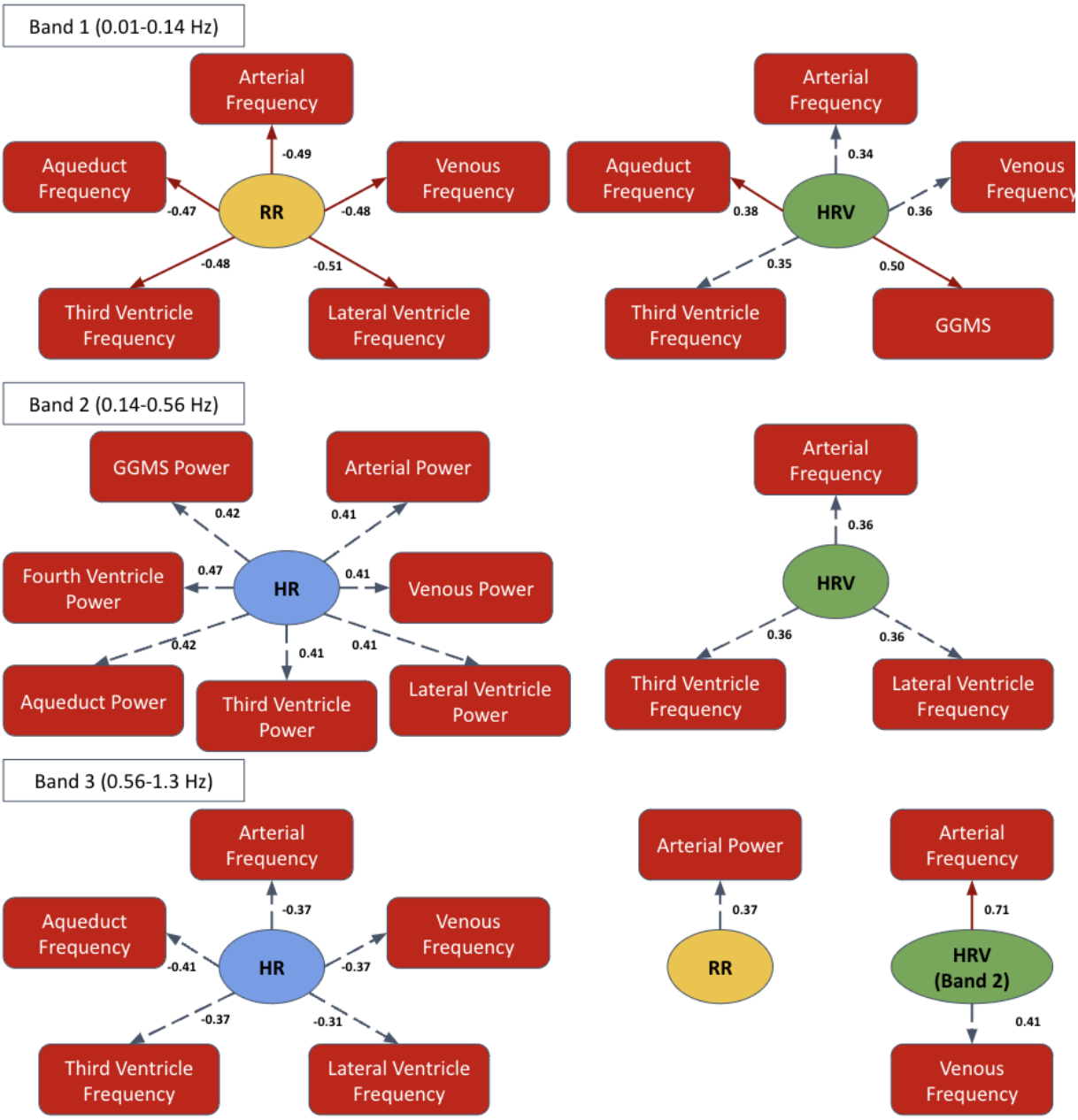

Figure 4. The contribution of multiple factors to BOLD and CSF velocity fluctuations in the Bands 1-3. Statistically significant effect sizes are shown as solid lines in the figure, with dashed arrows representing substantial but indeterminant associations ($p < 0.5$ but failed the bootstrapped test). The numbers displayed next to the arrows indicate the effect size. HR: heart rate; RR: respiratory rate; HRV: heart-rate variability; RVT: respiratory variability.

- Band 1: BOLD signal fluctuation frequency is positively associated with HRV and negatively associated with RR in arteries, veins, the lateral ventricle, third ventricle and aqueduct. No BOLD signal power associations are found.
- Band 2: No significant association is found between BOLD signal oscillation and physiological parameters (i.e. HR, RR, HRV, RVT). BOLD signal power is indeterminant positively associated with HR and frequency is positively associated with HRV for artery, lateral ventricle and third ventricle.
- Band 3: There was a significant association found between arterial BOLD signal fluctuation frequency and Band 2 HRV. Furthermore, there is a indeterminant negative association between BOLD fluctuation frequency and HR for all ROIs except the fourth ventricle and GGMS.

Thus, we also see obvious differences across the infraslow frequency bands. While Band 1 is more strongly driven by respiratory rate, Band 2 and 3, although insignificant, are driven more strongly by both HR. Interestingly, basal CO_2 was not a strong driver of the differences across capnic conditions.

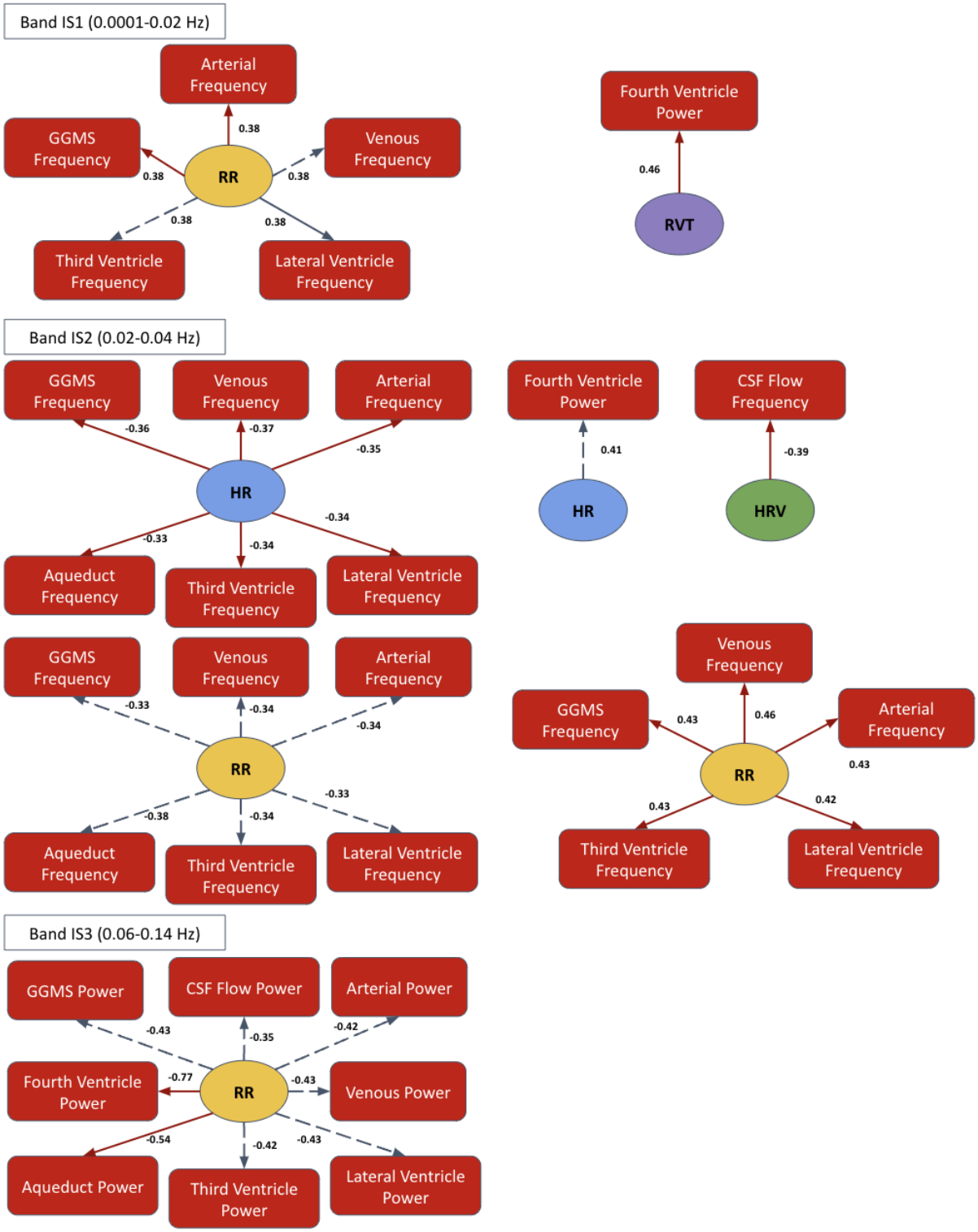

Figure 5. The contribution of multiple factors to BOLD and CSF velocity fluctuations in the infraslow Bands IS1-3. Statistically significant effect sizes are shown as solid lines in the figure, with dashed arrows representing substantial but indeterminant associations ($p < 0.5$ but failed the bootstrapped test). The

numbers displayed next to the arrows indicate the effect size. HR: heart rate; RR: respiratory rate; HRV: heart-rate variability; RVT: respiratory variability.

- Band IS1: There is a positive association between the BOLD signal fluctuation frequency and respiratory rate, which is significant in the artery and lateral ventricle ROIs, but not significant in vein and third ventricle ROIs. Moreover, BOLD signal fluctuation power is significantly positively associated with RVT in the fourth ventricle. There are also substantial indeterminant positive associations between CSF flow frequency and HR.
- Band IS2: There are numerous significant contributions by HR and RR to neurofluid dynamics in Band IS2. In all ROIs except the fourth ventricle and CSF flow, the BOLD signal fluctuation frequency is significantly and negatively associated with HR. The substantial negative association with respiratory rate is indeterminant. Meanwhile, BOLD signal fluctuation power is positively and significantly associated with RR in the ROIs listed above. In addition, we found a significant and negative association between CSF flow frequency and HRV.
- Band IS3: Respiratory rate shows significant negative associations with BOLD signal power in the aqueduct and fourth ventricle ROIs, as well as substantial indeterminant negative associations with BOLD signal power in the remaining ROIs.

We see obvious differences across the infraslow frequency bands. While Bands IS1 and IS3 are both more strongly driven by respiratory rate, Band IS2 is driven by both RR and HR. Interestingly, basal CO2 was not a strong driver of the differences across capnic conditions.

CRF and RRF for different capnic conditions

Based on the fact that HRV and RVT are the predominant mediators of the relationship between capnic condition and BOLD signal changes in neurofluid ROIs, we further estimated the response functions linking the BOLD data and these two variables for each capnic condition and ROI. As shown in **Figure 4**, arterial and venous CRFs behave very similarly. These in turn are similar to the CSF ROIs. The response is largely positive during HYC and negative during HOC, with NOR being the intermediate. HYC is generally associated with the highest positive CRF peak, and NOR with the highest negative CRF peak. Moreover, the responses for HOC and NOR are at a higher frequency than for HYC. The CRF from the GGMS exhibits a similar behavior to that of the BOLD signal obtained from neurofluid ROIs.

On the other hand, as shown in **Figure 5**, the majority of ROIs display positive initial peaks for RRF followed by an undershoot in the NOR and HOC conditions, with the exception of the RRF estimated from CSF flow, which shows a negative initial peak. Furthermore, while HOC displays larger RRFs and faster variations than NOR, HYC is associated with a very sluggish RRF with no noticeable undershoot. The RRFs for one subject were excluded from the plots due to outlier behaviour.

Interaction between BOLD and respiratory/cardiac variability time series

Lastly, the mutual information analysis did not reveal significant differences across capnic conditions. That is, the amount of mutual information between BOLD and HRV (or RVT) did not differ with capnia. There was, however, a trend of increasing mutual information for HRV and RVT from hypocapnia to hypercapnia in the case of the CSF flow velocity **(Fig. S2** in Supplementary Materials).

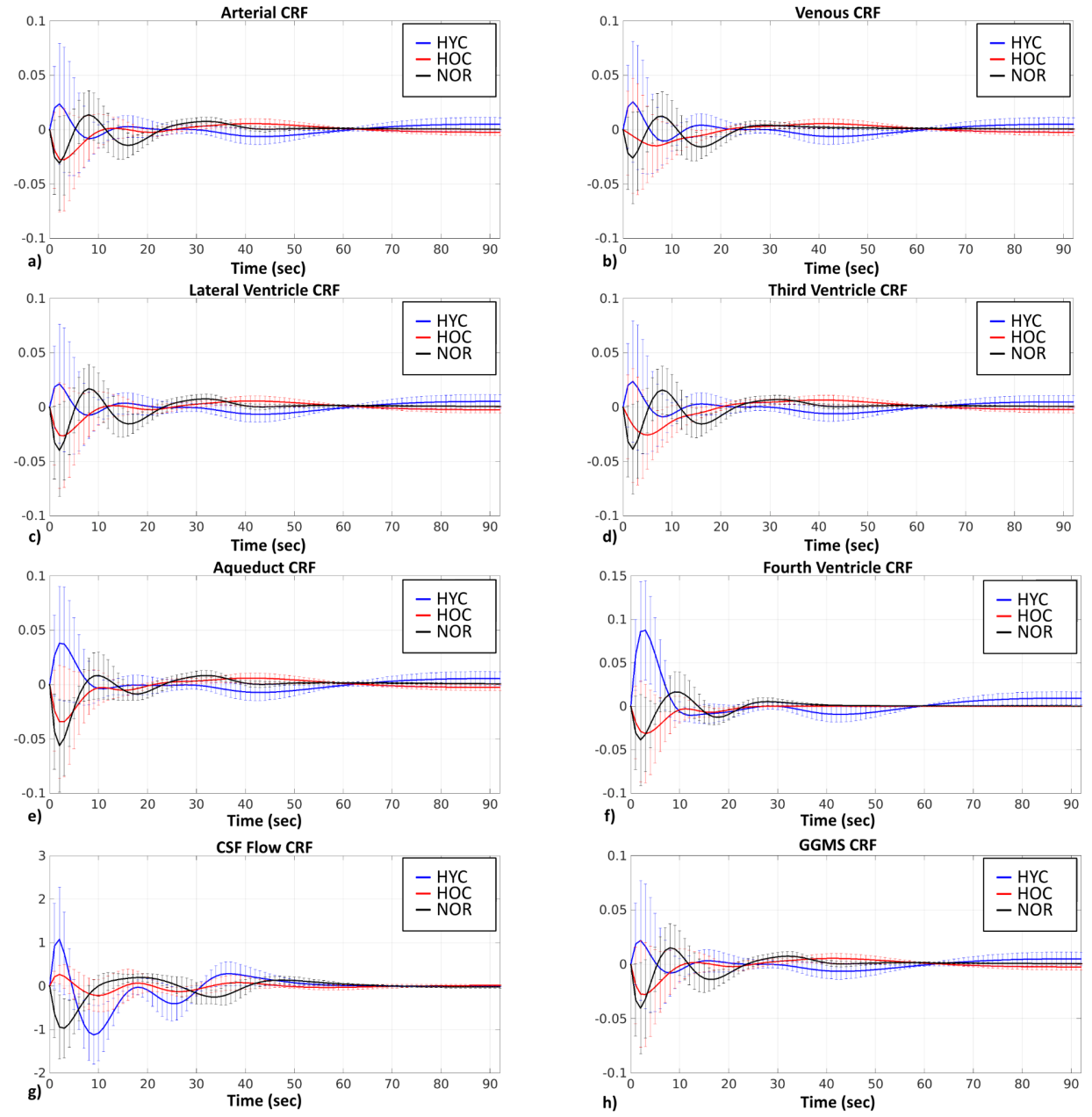

Figure 6. CRF across different capnias. All plots are shown as averages across subjects, and the error bars represent the standard deviation. HYC: hypercapnia; HOC: hypocapnia; NOR: normocapnia.

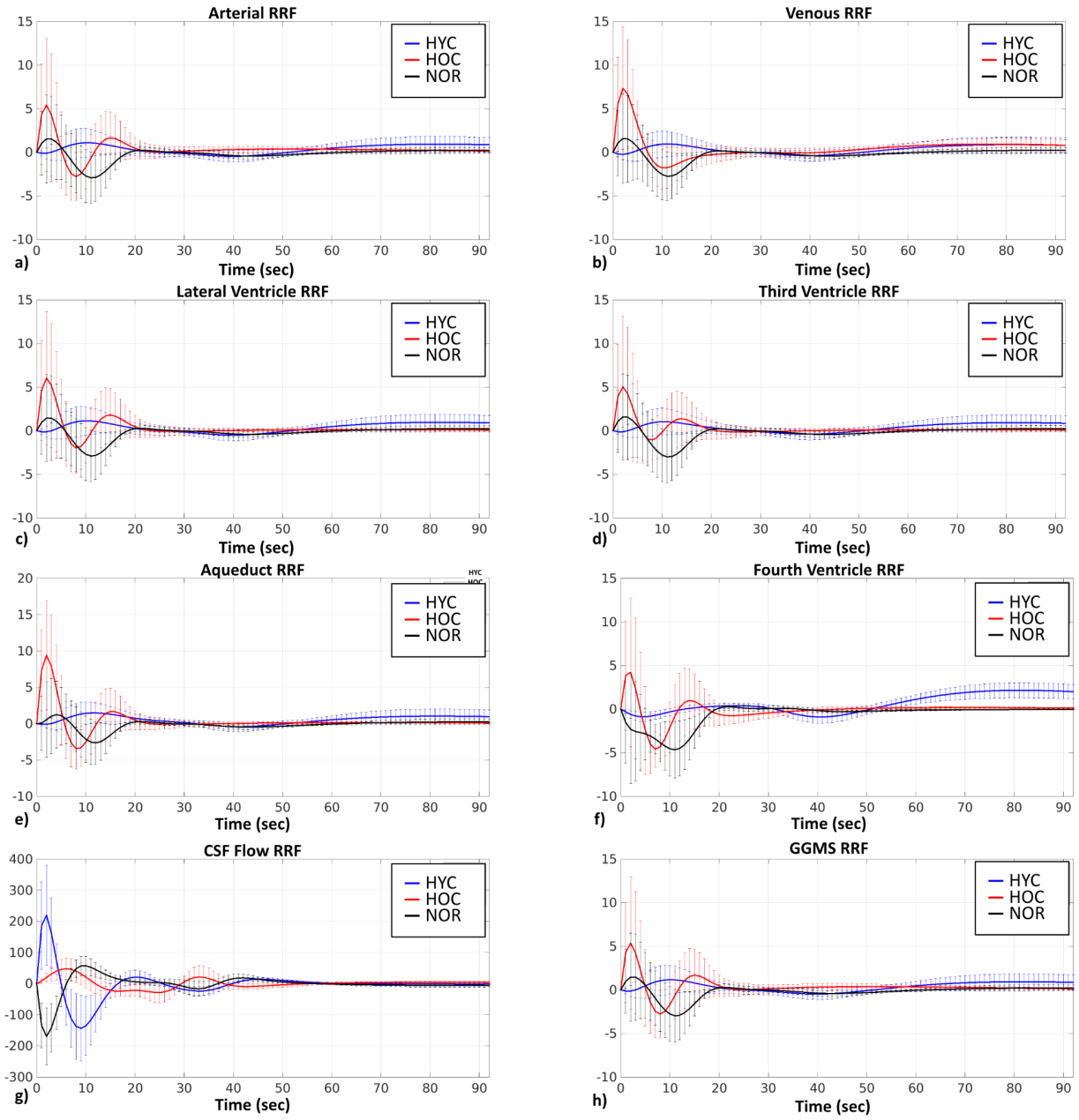

Figure 7. RRF across different capnias. All plots are shown as averages across subjects, and the error bars represent the standard deviation. HYC: hypercapnia; HOC: hypocapnia; NOR: normocapnia.

Discussion

In this work, we investigated the variations in neurofluid dynamics, as reflected in their rs-fMRI signals, across different capnic states. Our main findings are:

1. Neurofluid dynamics are consistent across the vascular and CSF systems at all capnic levels;
2. Relative to a normocapnic steady state, both hypocapnic and hypercapnic steady states are associated with increased BOLD signal power and shifts in BOLD signal frequency in vascular ROIs in a band-dependent manner;
3. Relative to hypocapnia, hypercapnia is associated with both increased and decreased BOLD signal power in vascular ROIs, depending on the frequency band;
4. These trends are largely reproduced in the CSF ROIs and in the CSF velocity dynamics.
5. These power and frequency variations across capnic conditions are mostly driven by respiratory and heart-rate differences rather than by steady-state CO_2; these behaviours are mirrored in the behaviour of the BOLD GGMS, and suggest an important role of the autonomic nervous system (ANS);
6. These variations in neurofluid dynamics can be explained by the differences in the fMRI cardiac and respiratory response functions, which suggest that the manner of ANS modulation of neurofluid flow varies with capnic condition.

The agreement in flow patterns across vascular and CSF regions as measured using BOLD fMRI is in agreement with our previous findings (Attarpour et al., 2021) as well as with based on cine phase contrast (ElSankari et al., 2013), and reflects the driving force of arterial flow in neurofluid circulation (Kedarasetti et al., 2020). Physiologically, manipulations of basal CO_2 can alter many things, including vascular tone, sympathetic nervous (SNS) function, breathing through chemoreflex control and cardiac pulsation rate through baroreflex control. Our findings disprove our first hypothesis, in that changes in vascular tone are not the main drivers of BOLD signal amplitude. They partly support our second hypothesis, since HR and RR appear to be strong drivers of BOLD signal frequency in multiple frequency bands. Importantly, our findings highlight the important role of the ANS in modulating neurofluid dynamics in response to changes in vascular physiology.

CO_2, heart and respiratory rate

While the group comparisons across capnic conditions did not reveal a significant difference in HR or RR, on an individual level, HR and RR may vary across conditions (**Figure S1** in Supplementary Materials). At a group level, while not significant, HR is higher at both hyper- and hypocapnia. As well, RR is highest at hypercapnia and lowest at hypocapnia. As our analyses are band-specific, frequency shifts due to such changes can result in seemingly counterintuitive observations. For example, an upward shift of the RR-related BOLD signal peak from Band 2 to Band 3 can result in a reduction in the central frequency in Band 3. Likewise, an upward shift of the HR-related BOLD signal peak can result in the aliasing of the HR peak into Band 1. Based on our HR measurements, this applies to 3 of the participants (**Fig. S1** in Supplementary Materials).

CO_2 and vascular tone

Capnia-related vascular tone was our first hypothesized mechanism for driving the BOLD signal amplitude and frequency. Vascular tone is defined as the contractile activity of vascular smooth muscle cells in the walls of small arteries and arterioles. In either hyper- or hypocapnia, vascular contractile activity could be more restricted in one direction, resulting in reduced vascular tone compared to normocapnia.

Previous work by Biswal et al. uncovered a suppression of 0.08 Hz band rs-fMRI signal fluctuations during 5% hypercapnia, which was attributed to the reduced sensitivity of hemodynamic modulation during a vasodilated state (Biswal et al., 1997). These observations can in part explain our own observations of significant positive correlations between rs-fMRI signal fluctuation amplitude and CVR, with CVR being diminished at hyper- and hypocapnia compared to normocapnia (Golestani et al., 2016). However, it was not entirely clear to what extent this was due solely to the effect of basal CO_2 on CVR, and due to the neuromodulatory effects of CO_2. Moreover, Peebles et al. supported the regulation of CVR by the sympathetic nervous system through the alpha1-adrenoreceptors (Peebles et al., 2012).

Previous work by Cohen et al. (E. R. Cohen et al., 2002) used hypocapnia and hypercapnia to alter basal CO_2 and found that the BOLD peak height was inversely correlated with basal CO_2, while the BOLD FWHM was directly correlated with basal CO_2. This was attributed to the effect of elevated CO_2 on the vasodilatory mechanisms that overcame the effect of increased flow velocity that led to the sluggish BOLD response at hypercapnia (E. R. Cohen et al., 2002). Work by Bailes et al. has shown that slower HRF is associated with higher rs-fMRI spectral power in the low-frequency band (Bailes et al., 2023). Moreover, the HRF shape is reportedly altered in aging (Fesharaki et al., 2023). The HRF shape should to some extent be encapsulated in the frequency content of the low-frequency BOLD signal.

Our previous work also showed that cerebrovascular reactivity (CVR) is reduced at hyper- and hypocapnia relative to normocapnia. As low-frequency (< 0.1 Hz) CSF signal variations have been conjectured to be driven by CBV variations (Fultz et al., 2019), the higher CVR at normocapnia may be associated with greater CSF fluctuations than at hyper- or hypocapnia. Additionally, compensatory changes in response to pH alterations during hyper- and hypocapnia exist in both CSF and blood, potentially through similar mechanisms (Feher, 2017). CSF volume is reduced during hyper- and hypocapnia (Grant et al., 1989), while parenchyma volume increases during hypercapnia (van der Kleij et al., 2020). Moreover, changes in MAP during hypercapnia and hypocapnia have been related to changes in CSF and venous (sagittal sinus) pressure (Hamer et al., 1974). CSF flow has been shown as the temporal derivative of the rs-fMRI time series during wakefulness (Yang et al., 2022). The frequency of CSF flow fluctuations and BOLD signal fluctuations can both increase with respiratory rate as part of hypercapnia and hypocapnia (Vinje et al., 2019).

Notwithstanding the established relationship between hemodynamics and CSF dynamics, the mechanisms through which basal CO_2 influences CSF dynamics are less well documented. Conceivably, basal CO_2 can affect CSF volume variability and CSF flow velocity as a result of vascular mechanisms stated above, but the extent to which this is the case is unclear. Following the vascular-tone mechanism of CO_2, we would expect that hypercapnia and hypocapnia, both associated with reduced vascular tone, be associated with reduced neurofluid fluctuation as well.

Interestingly, $PETCO_2$ did not appear to be directly associated with BOLD signal fluctuations and CSF flow power and frequency. Thus, our first hypothesis did not find support from the data.

CO_2 and neuronal activity

An alternate or complementary mechanism for the effect of CO_2 on FC is through the effect of CO_2 on neural activity. Aside from modulating vascular tone, hypercapnia has been shown to suppress EEG and MEG power in various frequency bands, suggesting a reduction in synchronous neuronal activity. Elevated CO_2 has been associated with suppressed steady-state amplitude of the band-limited EEG Hilbert envelope amplitude in multiple bands (Driver et al., 2016; F. Xu et al., 2011). By the same token, reduced CO_2 should be associated with enhanced EEG amplitude. In this regard, previous work suggests that neuronal activity variations can influence hemodynamics, which in turn influence CSF fluctuations as measured using BOLD rs-fMRI. Fultz et al. found that the global grey-matter BOLD signal was coupled with the CSF BOLD signal from the fourth ventricle, which was in turn coupled with low-frequency delta activity. This was used as evidence to demonstrate a link between global neuronal activity, blood oxygenation and CSF-based BOLD signal fluctuations (Fultz et al., 2019). Following the work of Fultz et al., if hypercapnia and hypocapnia act to suppress and enhance synchronized neuronal activity fluctuations, respectively, they can also enhance and suppress the CSF signal fluctuations, respectively. The GGMS originates from all grey matter and has also been associated with global activity, particularly within the low-frequency range (Band 1) (Bolt et al., 2022). In addition, other studies have revealed the physiological origins of the GGMS and further suggest that the global signal may be related to neurofluid flow (Fultz et al., 2019; Yang et al., 2022). Here, we confirm that what we observed in the neurofluid can be mirrored in the GGMS. However, the origins of the GGMS are far from clear. For instance, neural activity has been shown to entrain regional vasomotion (Drew et al., 2020; Mateo et al., 2017), while subdural vascular oscillations in the cranial bone has also been found to closely resemble the GMS (Huber et al., n.d.) suggesting that the GMS also contains systemic vascular oscillations (Tong et al., 2013).

Thus, while neuronal activity can indeed vary regionally with capnic conditions, assuming solely a neural driver of the BOLD signal variations that we observed would suggest that hypercapnia and hypocapnia should be associated with opposite effects relative to normocapnia. This was interestingly not the case, as seen in **Figure 2** and **Tables 3** and **4**. Thus, there must be other major drivers of the observed variations.

CO_2 and sympathetic tone: the role of the ANS

RR, HRV and RVT were found to significantly correlate with rs-fMRI signal fluctuation amplitude and frequency in neurofluid ROIs in the low-frequency band (Band 1 and Band IS1-3), as well with rs-fMRI-derived CSF flow velocity fluctuations. This is particularly true after performing motion regression. Changes in RR, HR, RVT and HRV can also alter not only the signal fluctuation amplitude but also the frequencies of their corresponding fMRI signal components, and result in altered frequency content in specific bands of rs-fMRI signal (Birn et al., 2006; Chang et al., 2009).

RR, HR, RVT and HRV are key parameters reflecting ANS function (Chang et al., 2013; Lane et al., 2009; Lehrer & Gevirtz, 2014; Napadow et al., 2008). An important part of ANS

function, the sympathetic tone is directly correlated with the level of sympathetic activity, and the influence on vascular oscillations is complex. As part of the sympathetic reflex, levels of CO_2 and O_2 in the blood are monitored by chemoreceptors in the brainstem and carotid bodies. Increased CO_2 or decreased O_2 levels trigger the sympathetic nervous system (SNS) to increase RR and HR to maintain proper gas exchange (Davis et al., 1977), thereby modulating RVT and leading to reduced HRV. On the other hand, elevated SNS tone triggers the release of norepinephrine from sympathetic nerve endings near blood vessels. Norepinephrine binds to alpha-adrenergic receptors on smooth muscle cells in the blood vessel walls, causing them to contract. This vasoconstriction also leads to increased MAP (Smith & Maani, 2023) and reduced blood flow (CBF) as well as volume (CBV). In the brain, this vasoconstriction may also divert blood towards the heart and limbs, except for in regions related to the stress response (ter Laan et al., 2013). We did not monitor blood pressure (MAP) during our capnic conditions, so we cannot comment on the role of the vagal reflex in inducing RR and HR changes. Moreover, a recent study suggests a negative correlation between SNS activity and peripheral vasomotion in anticipation of pain stimuli (Z. Xu et al., 2024). Thus, the pathways of ANS influence can be summarized as: increased CO_2->increased SNS tone->reduced CBF and CBV->reduced vasomotion.

The non-infraslow band and basal CO_2

In this study, we used the rs-fMRI signal in vascular and CSF ROIs as a surrogate for neurofluid flow. Our ROI definition does not preclude the possibility of partial-volume effects with subcortical brain tissue, but the main mechanism of BOLD signal change in arterial CSF regions is thought to be inflow effects (Diorio et al., 2023; Fultz et al., 2019). This is particularly true for the third ventricle, fourth ventricle and cerebral aqueduct, less so for the lateral ventricles, as we showed in our previous work (Attarpour et al., 2021). Interestingly, in this study, the signal variations in the lateral ventricle tend to mirror those of the other neurofluid regions. In large veins, the BOLD signal fluctuations are largely attributable to T2 variations, which, also as shown in our previous work (Attarpour et al., 2021), demonstrate patterns similar to those in large arteries.

Band 1 is the most commonly used for FC analysis, its power and frequency can be linked to patterns of neural activity as measured using EEG, as demonstrated in our recent study on normal aging (X. Z. Zhong & Chen, 2022). This low-frequency band (< 0.1 Hz) of the rs-fMRI signal is also typically chosen to represent vascular and CSF dynamics (Yang et al., 2022). There are additionally low-frequency physiological processes such as HRV and RVT that contribute to Band 1 BOLD signal dynamics. In our case, since $PETCO_2$ is fixed, it negligibly contributes to the signal. In contrast, given our high sampling rate, Bands 2 and 3 generally reflect respiratory and cardiac activity and are less associated with neural activity, although recent work suggests otherwise (Chen et al., 2021; Chen & Glover, 2015).

According to **Figure 4**, even though the outcomes of BOLD power comparisons between hypercapnia and hypocapnia vary across the non-infraslow frequency bands, we found that normocapnia was always associated with the lowest signal power. This seems to contradict findings from previous research that suggested hypercapnia imparts lower signal power than normocapnia (Biswal et al., 1997). However, the methodology employed in this study differs significantly from that used by Biswal et al; this study utilized fixed end-tidal CO_2 at each capnic level whereas Biswal et al. utilized free breathing; significant differences between BOLD signals

from these two methodologies were demonstrated in a recent study (Kish et al., 2023). Moreover, unlike in our previous work (Attarpour et al., 2021), we used motion regression in addition to motion coregistration to ensure the findings are minimally driven by capnia-specific head motion.

The seminal work of Biswal et al. (Biswal et al., 1997) did not involve the higher frequencies (i.e. Bands 2 and 3). In our work, we observe no significant association between BOLD oscillation power and high-frequency physiological signals such as HR and RR (**Fig. 4**), although HR and HRV (high-frequency HRV) were prominently figured as potential modulators of BOLD signal power and frequency in Band 2, respectively. Band 2 HRV continues to influence BOLD signal frequency in Band 3 along with HR. Due to the fact that we are focusing on neurofluid ROIs, we expect minimal contributions of regional neural activity to these patterns in BOLD signal power. Rather, as discussed in the section *CO_2 and Sympathetic Tone,* we expect that changes in RR, HR, RVT and HRV can alter the signal fluctuation amplitudes of their corresponding signal components in fMRI.

BOLD signal frequency and power differences across capnic conditions are likely governed by different mechanisms and thus can be expected to display different levels of sensitivity to the capnic condition. BOLD signal frequency in Band 1 is significantly associated with RR, while HRV, as a surrogate of ANS activity, modulates the frequency of the rs-fMRI oscillations across all three non-infraslow frequency bands. This is also reflected in the CRF and RRF estimates. Since the technique for estimating the RRF (Birn et al., 2006) and CRF (Chang et al., 2009) were proposed, there have been reports demonstrating the spatial heterogeneity in these physiological response functions (Chen et al., 2020; Falahpour et al., 2013; Golestani et al., 2015). In this work, we further demonstrate that these response functions vary by capnic condition. The CRF is largely negative during HOC and positive during HYC, with NOR displaying an intermediate shape; this is consistent across all ROIs. The shape of the CRF during NOR is consistent with the inverse of the CRF found (in response to HR variations instead of HRV) by Chen et al. (Chen et al., 2020) in the vicinity of large veins in resting state. The fact that the polarity of the CRF shifts gradually from HOC to HYC suggests a role of SNS tone in influencing neurofluid dynamics, as described earlier in the section titled *CO_2 and Sympathetic Tone*. This is also consistent with the trend of mutual information shift from HOC to HYC. Conversely, our estimates of RRF are similar to those from Chen et al. but only in the HOC and NOR conditions. The HYC is associated with a very slowly varying RRF, which is reminiscent of the slowly-varying BOLD response that Cohen et al. observed during a hypercapnic baseline (E. R. Cohen et al., 2002). Thus, our results demonstrate that the manner in which HRV and RVT modulate neurfluid dynamics also varies by capnia. More importantly, these results clarify the manner in which neurofluid dynamic in the low-frequency band differs across capnic conditions. More broadly, different individuals can be found on different points on the capnic spectrum, basal capnia is also an important contributor to inter-subject and inter-session variability in CRF and RRF, as well as in neurofluid flow patterns.

Specific to Bands 3, ANS involvement in the frequency variations is more difficult to understand since low-frequency ANS-surrogate metrics such as HRV and RVT (Jerath et al., 2006; Naifeh et al., 1982) may not directly feed into this band, but may exert indirect modulatory effects (Hales, 1733). That is, one can modulate one's HR and thereby HRV by modifying one's breathing pattern (including RR and RVT). It is evident that Band 2 oscillatory frequency across all neurofluid ROIs is driven by HRV. Intriguingly, Band 3 oscillatory frequency is negatively

correlated with HR for most ROIs and negatively correlated with Band 2 HRV for vascular ROIs; this is intriguing, given that higher HR should contribute to higher BOLD frequency in Band 3. Such an observation may be explained by the aliasing of high HR peaks into Band 1, and a shift of HRV-related power from Band 2 into Band 3. Furthermore, through neurofeedback, it is possible that HRV (located in Band 1 and 2), as well as RVT (power mainly in Band 1), can influence the BOLD signal at higher frequency bands by influencing HR (Lehrer & Gevirtz, 2014; Schwartz & Beatty, 1977).

The infra-slow band and basal CO_2

The low-frequency band (< 0.1 Hz) of the BOLD signal can be further divided into several infra-slow vascular frequencies guided by previous work on infraslow hemodynamics. These form an interesting aspect of neurofluid flow that is also affected by basal CO_2. As the term implies, infra-slow vascular oscillations are defined as spontaneous low-frequency oscillations originating from the microvasculature. Researchers have used functional near-infrared spectroscopy (fNIRS) to identify three major sources of infraslow vascular oscillations (Bracic & Stefanovska, 1998): endogenic oscillations (0.003-0.02 Hz); neurogenic oscillations (0.02-0.04 Hz); and myogenic oscillations (0.04-0.15 Hz) (Ainslie & Duffin, 2009; Truong et al., 2022).

- Band IS1: Endogenous oscillations stem from metabolic activity of the endothelium in the microvasculature, which further stimulates vasodilation and vasoconstriction and alters vascular tone as well (see section titled *Vascular Tone*) (Rubanyi, 1991). As described previously, we expect reduced vascular tone during hyper- and hypocapnia to be associated with reduced endogenous oscillatory power. However, this is not the case, as both hyper- and hypocapnia are associated with a higher power in Band IS1 (**Figure. 3** and **Table 2**)
- Band IS2: Neurogenic oscillation is associated with intrinsic neuronal activity, which is in turn associated with sympathetic and parasympathetic nerve activity (see above sympathetic tone section) (Ainslie & Duffin, 2009). As described previously, we expect increased SNS tone during hypercapnia and the opposite during hypocapnia to modulate power in Band IS2 accordingly. This, however, was not the case, as BOLD signal power was generally highest for hypocapnia with minimal difference between normo- and hypercapnia.
- Band IS3: Myogenic oscillation reflects the activity of the smooth muscles in the vasculature. The smooth muscles in vascular smooth muscles would relax during hypercapnia, and small vessels would be the most responsive to this condition (Stefanovska & Krošelj, 1997; Wasserman & Patterson, 1961). In this case, we would expect a similar signal variation pattern as predicted for Band IS1, but this was also not the case.

Increased myogenic oscillations have been associated with the activation of K^+ channels with a hypercapnia-induced low pH, which in turn leads to hyperpolarization of endothelial cells and smooth muscle cells (Ainslie & Duffin, 2009). Moreover, an important recent discovery that MAP pulsations can directly modulate neuronal activity (Jammal Salameh et al., 2024) suggests interactions between neurogenic and myogenic oscillations. In addition to spontaneous

oscillations of the vascular bed, infraslow oscillations may also result from low and very low-frequency RR-interval oscillations (~20% of respiratory frequency peak), which may be related to cardiac health conditions and also associated with sympathetic tone (also see above section titled *CO_2 and sympathetic tone*) (Taylor et al., 1998). It is, however, unclear to what extent these RR-interval oscillations may contribute to the infraslow oscillations observed in rs-fMRI.

The RR affects all three infraslow bands. It affects Band IS1 through frequency, Band IS3 through power and Band IS2 through both frequency and power (**Fig. 5**), but the mechanism is unclear. An obvious reason may be the shift in RR-related signal power peak as described in the section titled *CO_2, Heart and Respiratory Rate*. There are, however, two reasons against such a theory. First, if the BOLD oscillation frequency and power changed due to the RR peak shift, we are unlikely to observe a frequency decrease and power increase in Band IS2 in conjunction with a frequency increase in Band IS1, suggesting that some BOLD signal components have shifted into IS2 from IS1. Moreover, the BOLD signal power spectra from a previous study (Tong et al., 2019) suggest that the RR peak power would be lower than the peak power of low-frequency oscillation in Band 1 (also as shown in **Fig. 2**). Thus the spread of RR peak into the lower frequency bands is unlikely to dominate the oscillation variations in the infraslow bands.

Limitations

One of the major limitations of this study may be the limited number of participants. However, although our dataset provides unique insight into the physiological activity behind different capnias, only 13 participants were included, which undermines the generalizability of the results from linear mixed effect models. Further, we used a relatively low spatial resolution in order to maximize the sampling rate, which may lead to partial-volume effects in our analysis. As a result of the same reason, aqueduct and fourth ventricle analysis may not be available to all participants due to a limited field of view (also see *method* section). The repetition time (TR=380 ms) we used, despite our efforts to maximize the sampling rate, still poses a challenge to capture all cardiac harmonics.

In our study, we chose ROIs that are distant from the local specific neural activity, such as macrovascular and CSF ROIs. In spite of this, the impact of the capnic on global activity cannot be entirely ignored (F. Xu et al., 2011). There is a possibility that variations in global neural activity and HRV can be transmitted into macrovasculature, which supplies and drains brain blood. In our linear-mixed effect model, these factors have not been included. In addition, some other factors, such as vasomotion and vascular tone, may be difficult to monitor and have not been incorporated into the linear mixed effect model. It is also noteworthy that the macrovascular ROIs used in this study are based on regions with high BOLD power, which may differ from real macrovascular structures based on recent biophysical models (X. Zhong et al., 2024).

The physiological recording provides insight into cardiac and respiratory activity, and we used them as a surrogate for the activity of the autonomic nervous system. Numerous studies have demonstrated the link between cardiac activity and respiratory activity and ANS activity, however, the modulation of such activities depends on far more than ANS activity alone (Gordan et al., 2015), and such indirect relationships may not exactly replicate ANS activation. On the basis of factors such as healthy young participants and the short capnic period, the ANS appears to be the most likely pathway for cardiac and respiratory variation.

Conclusions

The study of neurofluid dynamics using in-vivo imaging is an exciting new avenue of research that provides important insights into waste clearance and neuronal signalling in the brain. In this work, we investigate the relationship between capnic condition and neurofluid dynamics as measured by BOLD rs-fMRI signal fluctuations. Inducing different levels of basal CO_2 has well-established effects on cerebrovasculature, which are in turn linked to the flow of CSF. However, in this study, we found this link is mediated by autonomic activity. Moreover, we found that neurofluid dynamics are very similar to those of the global mean signal. We believe these findings can provide new insights into the regulation of neurofluid flow, especially of CSF flow.

Acknowledgments

The authors would like to acknowledge financial support from Canadian Institutes of Health Research and the Canada Research Chairs Program (JJC) and funding support from Ydessa Hendeles Graduate Scholarship (XZZ).

Reference

Ainslie, P. N., & Duffin, J. (2009). Integration of cerebrovascular CO2 reactivity and chemoreflex control of breathing: mechanisms of regulation, measurement, and interpretation. *AJP: Regulatory, Integrative and Comparative Physiology*, *296*(5), R1473–R1495.

Akselrod, S., Gordon, D., Ubel, F. A., Shannon, D. C., Berger, A. C., & Cohen, R. J. (1981). Power spectrum analysis of heart rate fluctuation: a quantitative probe of beat-to-beat cardiovascular control. *Science*, *213*(4504), 220–222.

Attarpour, A., Ward, J., & Chen, J. J. (2021). Vascular origins of low-frequency oscillations in the cerebrospinal fluid signal in resting-state fMRI: Interpretation using photoplethysmography. *Human Brain Mapping*, *42*(8), 2606–2622.

Bailes, S. M., Gomez, D. E. P., Setzer, B., & Lewis, L. D. (2023). Resting-state fMRI signals contain spectral signatures of local hemodynamic response timing. *eLife*, *12*. https://doi.org/10.7554/eLife.86453

Birn, R. M., Diamond, J. B., Smith, M. A., & Bandettini, P. A. (2006). Separating respiratory-variation-related fluctuations from neuronal-activity-related fluctuations in fMRI. *NeuroImage*, *31*(4), 1536–1548.

Biswal, B., Hudetz, A. G., Yetkin, F. Z., Haughton, V. M., & Hyde, J. S. (1997). Hypercapnia reversibly suppresses low-frequency fluctuations in the human motor cortex during rest using echo-planar MRI. *Journal of Cerebral Blood Flow and Metabolism: Official Journal of the International Society of Cerebral Blood Flow and Metabolism*, *17*(3), 301–308.

Bolt, T., Nomi, J. S., Bzdok, D., Salas, J. A., Chang, C., Thomas Yeo, B. T., Uddin, L. Q., & Keilholz,

S. D. (2022). A parsimonious description of global functional brain organization in three spatiotemporal patterns. *Nature Neuroscience*, *25*(8), 1093–1103.

Bracic, M., & Stefanovska, A. (1998). Wavelet-based analysis of human blood-flow dynamics. *Bulletin of Mathematical Biology*, *60*(5), 919–935.

Calhoun, V. D., Adali, T., Pearlson, G. D., & Pekar, J. J. (2001). A method for making group inferences from functional MRI data using independent component analysis. *Human Brain Mapping*, *14*(3), 140–151.

Chang, C., Cunningham, J. P., & Glover, G. H. (2009). Influence of heart rate on the BOLD signal: the cardiac response function. *NeuroImage*, *44*, 857–869.

Chang, C., Metzger, C. D., Glover, G. H., Duyn, J. H., Heinze, H.-J., & Walter, M. (2013). Association between heart rate variability and fluctuations in resting-state functional connectivity. *NeuroImage*, *68*, 93–104.

Chen, J. E., & Glover, G. H. (2015). BOLD fractional contribution to resting-state functional connectivity above 0.1 Hz. *NeuroImage*, *107*, 207–218.

Chen, J. E., Glover, G. H., Fultz, N. E., Rosen, B. R., Polimeni, J. R., & Lewis, L. D. (2021). Investigating mechanisms of fast BOLD responses: the effects of stimulus intensity and of spatial heterogeneity of hemodynamics. *NeuroImage*, *118658*, 118658.

Chen, J. E., Lewis, L. D., Chang, C., Tian, Q., Fultz, N. E., Ohringer, N. A., Rosen, B. R., & Polimeni, J. R. (2020). Resting-state "physiological networks." *NeuroImage*, *213*, 116707.

Cohen, E. R., Ugurbil, K., & Kim, S.-G. (2002). Effect of basal conditions on the magnitude and dynamics of the blood oxygenation level-dependent fMRI response. *Journal of Cerebral Blood Flow and Metabolism: Official Journal of the International Society of Cerebral Blood*

Flow and Metabolism, *22*(9), 1042–1053.

Cohen, J. (1977). *Statistical Power Analysis for the Behavioral Sciences (Revised Edition)*. Academic Press.

Davis, A. L., McCloskey, D. I., & Potter, E. K. (1977). Respiratory modulation of baroreceptor and chemoreceptor reflexes affecting heart rate through the sympathetic nervous system. *The Journal of Physiology*, *272*(3), 691–703.

Diorio, T. C., Vijayakrishnan Nair, V., Patel, N., Hedges, L. E., Rayz, V. L., & Tong, Y. (2023). Real-time Quantification of in vivo cerebrospinal fluid velocity using fMRI inflow effect. *bioRxiv.org: The Preprint Server for Biology*. https://doi.org/10.1101/2023.08.14.553250

Drew, P. J., Mateo, C., Turner, K. L., Yu, X., & Kleinfeld, D. (2020). Ultra-slow Oscillations in fMRI and Resting-State Connectivity: Neuronal and Vascular Contributions and Technical Confounds. *Neuron*, *107*(5), 782–804.

Driver, I. D., Whittaker, J. R., Bright, M. G., Muthukumaraswamy, S. D., & Murphy, K. (2016). Arterial CO2 Fluctuations Modulate Neuronal Rhythmicity: Implications for MEG and fMRI Studies of Resting-State Networks. *The Journal of Neuroscience: The Official Journal of the Society for Neuroscience*, *36*(33), 8541–8550.

ElSankari, S., Balédent, O., van Pesch, V., Sindic, C., de Broqueville, Q., & Duprez, T. (2013). Concomitant analysis of arterial, venous, and CSF flows using phase-contrast MRI: a quantitative comparison between MS patients and healthy controls. *Journal of Cerebral Blood Flow and Metabolism: Official Journal of the International Society of Cerebral Blood Flow and Metabolism*, *33*(9), 1314–1321.

Falahpour, M., Refai, H., & Bodurka, J. (2013). Subject specific BOLD fMRI respiratory and

cardiac response finctions obtained from global signal. *NeuroImage*, *72*, 252–264.

Feher, J. (2017). 6.6 - Control of Ventilation. In J. Feher (Ed.), *Quantitative Human Physiology: An Introduction*. Academic Press.

Fesharaki, N. J., Taylor, A., Mosby, K., Kim, J. H., & Ress, D. (2023). Global effects of aging on the hemodynamic response function in the human brain. *Research Square*. https://doi.org/10.21203/rs.3.rs-3299293/v1

Fultz, N. E., Bonmassar, G., Setsompop, K., Stickgold, R. A., Rosen, B. R., Polimeni, J. R., & Lewis, L. D. (2019). Coupled electrophysiological, hemodynamic, and cerebrospinal fluid oscillations in human sleep. *Science* , *366*(6465). https://doi.org/10.1126/science.aax5440

Golestani, A. M., Chang, C., Kwinta, J. B., Khatamian, Y. B., & Jean Chen, J. (2015). Mapping the end-tidal CO2 response function in the resting-state BOLD fMRI signal: Spatial specificity, test–retest reliability and effect of fMRI sampling rate. *NeuroImage*, *104*, 266–277.

Golestani, A. M., Kwinta, J. B., Strother, S. C., Khatamian, Y. B., & Chen, J. J. (2016). The association between cerebrovascular reactivity and resting-state fMRI functional connectivity in healthy adults: The influence of basal carbon dioxide. *NeuroImage*, *132*, 301–313.

Gordan, R., Gwathmey, J. K., & Xie, L.-H. (2015). Autonomic and endocrine control of cardiovascular function. *World Journal of Cardiology*, *7*(4), 204–214.

Grant, R., Condon, B., Patterson, J., Wyper, D. J., Hadley, M. D., & Teasdale, G. M. (1989). Changes in cranial CSF volume during hypercapnia and hypocapnia. *Journal of Neurology, Neurosurgery, and Psychiatry*, *52*(2), 218–222.

Halani, S., Kwinta, J. B., Golestani, A. M., Khatamian, Y. B., & Chen, J. J. (2015). Comparing

cerebrovascular reactivity measured using BOLD and cerebral blood flow MRI: The effect of basal vascular tension on vasodilatory and vasoconstrictive reactivity. *NeuroImage*, *110*, 110–123.

Hales, S. (1733). *Statical Essays: Statical Essays: Containing Hæmastaticks : Or, An Account*. Google Books. https://books.google.com/books/about/Statical_Essays.html?id=EtBaAAAAcAAJ

Hamer, J., Alberti, E., & Hoyer, S. (1974). Effects of arterial hypoxaemia, hypercapnia, and changes in cerebral perfusion pressure on mean cerebrospinal fluid and sagittal sinus pressure. *Acta Neurochirurgica*, *30*(3-4). https://doi.org/10.1007/BF01405576

Hedges, L. V. (1981). Distribution Theory for Glass's Estimator of Effect size and Related Estimators. *Journal of Educational and Behavioral Statistics: A Quarterly Publication Sponsored by the American Educational Research Association and the American Statistical Association*, *6*(2), 107–128.

Holland, A., & Aboy, M. (2009). A novel recursive Fourier transform for nonuniform sampled signals: application to heart rate variability spectrum estimation. *Medical & Biological Engineering & Computing*, *47*(7), 697–707.

Huber, D., Rabl, L., Orsini, C., Labek, K., & Viviani, R. (n.d.). *The fMRI global signal and its association with the signal from cranial bone*. Retrieved April 5, 2024, from https://www.biorxiv.org/content/10.1101/2024.03.27.587003v1.full.pdf

Jammal Salameh, L., Bitzenhofer, S. H., Hanganu-Opatz, I. L., Dutschmann, M., & Egger, V. (2024). Blood pressure pulsations modulate central neuronal activity via mechanosensitive ion channels. *Science*, *383*(6682), eadk8511.

Jerath, R., Edry, J. W., Barnes, V. A., & Jerath, V. (2006). Physiology of long pranayamic breathing: neural respiratory elements may provide a mechanism that explains how slow deep breathing shifts the autonomic nervous system. *Medical Hypotheses*, *67*(3), 566–571.

Johnson, P. C. (1991). The Myogenic Response. *Physiology* , *6*(1), 41–42.

Kastrup, J., Bülow, J., & Lassen, N. A. (1989). Vasomotion in human skin before and after local heating recorded with laser Doppler flowmetry. A method for induction of vasomotion. *International Journal of Microcirculation, Clinical and Experimental / Sponsored by the European Society for Microcirculation*, *8*(2), 205–215.

Kedarasetti, R. T., Drew, P. J., & Costanzo, F. (2020). Arterial pulsations drive oscillatory flow of CSF but not directional pumping. *Scientific Reports*, *10*(1), 10102.

Kety, S. S., & Schmidt, C. F. (1948). THE EFFECTS OF ALTERED ARTERIAL TENSIONS OF CARBON DIOXIDE AND OXYGEN ON CEREBRAL BLOOD FLOW AND CEREBRAL OXYGEN CONSUMPTION OF NORMAL YOUNG MEN. *The Journal of Clinical Investigation*, *27*(4), 484–492.

Kish, B., Chen, J. J., & Tong, Y. (2023). Effects of clamping end-tidal CO2 on neurofluidic low-frequency oscillations. *NMR in Biomedicine*, e5084.

Lane, R., McCrae, K., Reiman, E., Chen, K., Ahern, G., & Thayer, J. (2009). Neural correlates of heart rate variability during emotion. *NeuroImage*, *44*, 213–222.

Lehrer, P. M., & Gevirtz, R. (2014). Heart rate variability biofeedback: how and why does it work? *Frontiers in Psychology*, *5*, doi.org/10.3389/fpsyg.2014.00756.

Lumb, A. B. (2017). *Nunn's Applied Respiratory Physiology*. Elsevier.

Marshall, O., Uh, J., Lurie, D., Lu, H., Milham, M. P., & Ge, Y. (2015). The influence of mild

carbon dioxide on brain functional homotopy using resting-state fMRI. *Human Brain Mapping*, *36*(10). https://doi.org/10.1002/hbm.22886

Mateo, C., Knutsen, P. M., Tsai, P. S., Shih, A. Y., & Kleinfeld, D. (2017). Entrainment of Arteriole Vasomotor Fluctuations by Neural Activity Is a Basis of Blood-Oxygenation-Level-Dependent "Resting-State" Connectivity. *Neuron*, *96*(4), 936–948.e3.

Naifeh, K. H., Kamiya, J., & Sweet, D. M. (1982). Biofeedback of alveolar carbon dioxide tension and levels of arousal. *Biofeedback and Self-Regulation*, *7*(3), 283–299.

Napadow, V., Dhond, R., Conti, G., Makris, N., Brown, E. N., & Barbieri, R. (2008). Brain correlates of autonomic modulation: combining heart rate variability with fMRI. *NeuroImage*, *42*, 169–177.

Norcliffe, L. J., Rivera-Ch, M., Claydon, V. E., Moore, J. P., Leon-Velarde, F., Appenzeller, O., & Hainsworth, R. (2005). Cerebrovascular responses to hypoxia and hypocapnia in high-altitude dwellers. *The Journal of Physiology*, *566*(Pt 1), 287–294.

Peebles, K. C., Ball, O. G., MacRae, B. A., Horsman, H. M., & Tzeng, Y. C. (2012). Sympathetic regulation of the human cerebrovascular response to carbon dioxide. *Journal of Applied Physiology* , *113*(5). https://doi.org/10.1152/japplphysiol.00614.2012

Prokopiou, P. C., Pattinson, K. T. S., Wise, R. G., & Mitsis, G. D. (2018). Modeling of dynamic cerebrovascular reactivity to spontaneous and externally induced CO2 fluctuations in the human brain using BOLD-fMRI. *NeuroImage*. https://doi.org/10.1016/j.neuroimage.2018.10.084

Reivich, M. (1964). ARTERIAL PCO2 AND CEREBRAL HEMODYNAMICS. *The American Journal of Physiology*, *206*, 25–35.

Rubanyi, G. M. (1991). Endothelium-derived relaxing and contracting factors. *Journal of Cellular Biochemistry*, *46*(1), 27–36.

Sawilowsky, S. S. (2009). New Effect Size Rules of Thumb. *Journal of Modern Applied Statistical Methods: JMASM*, *8*(2), 26.

Schwartz, G. E., & Beatty, J. (1977). *Biofeedback, Theory and Research*.

Shams, S., Prokopiou, P., Esmaelbeigi, A., Mitsis, G. D., & Chen, J. J. (2022). Modeling the dynamics of cerebrovascular reactivity to carbon dioxide in fMRI under task and resting-state conditions. *NeuroImage*, *265*, 119758.

Slessarev, M., Han, J., Mardimae, A., Prisman, E., Preiss, D., Volgyesi, G., Ansel, C., Duffin, J., & Fisher, J. A. (2007). Prospective targeting and control of end-tidal CO2 and O2 concentrations. *The Journal of Physiology*, *581*(Pt 3), 1207–1219.

Smith, M. D., & Maani, C. V. (2023). Norepinephrine. In *StatPearls [Internet]*. StatPearls Publishing.

Song, A. K., Hett, K., Eisma, J. J., McKnight, C. D., Elenberger, J., Stark, A. J., Kang, H., Yan, Y., Considine, C. M., Donahue, M. J., & Claassen, D. O. (2023). Parasagittal dural space hypertrophy and amyloid-β deposition in Alzheimer's disease. *Brain Communications*, *5*(3), fcad128.

Stefanovska, A., & Krošelj, P. (1997). Correlation Integral and Frequency Analysis of Cardiovascular Functions. *Open Systems and Information Dynamics*, *4*(4), 457–478.

Taoka, T., & Naganawa, S. (2020). Neurofluid Dynamics and the Glymphatic System: A Neuroimaging Perspective. *Korean Journal of Radiology: Official Journal of the Korean Radiological Society*, *21*(11), 1199.

Taylor, J. A., Carr, D. L., Myers, C. W., & Eckberg, D. L. (1998). Mechanisms underlying very-low-frequency RR-interval oscillations in humans. *Circulation*, *98*(6), 547–555.

ter Laan, M., van Dijk, J. M. C., Elting, J. W. J., Staal, M. J., & Absalom, A. R. (2013). Sympathetic regulation of cerebral blood flow in humans: a review. *British Journal of Anaesthesia*, *111*(3), 361–367.

Tong, Y., Hocke, L. M., & Frederick, B. B. (2019). Low Frequency Systemic Hemodynamic "Noise" in Resting State BOLD fMRI: Characteristics, Causes, Implications, Mitigation Strategies, and Applications. *Frontiers in Neuroscience*, *13*, 787.

Tong, Y., Hocke, L. M., Nickerson, L. D., Licata, S. C., Lindsey, K. P., & Frederick, B. D. (2013). Evaluating the effects of systemic low frequency oscillations measured in the periphery on the independent component analysis results of resting state networks. *NeuroImage*, *76*, 202–215.

Truong, N. C. D., Wang, X., Wanniarachchi, H., & Liu, H. (2022). Enhancement of frequency-specific hemodynamic power and functional connectivity by transcranial photobiomodulation in healthy humans. *Frontiers in Neuroscience*, *16*, 896502.

van der Kleij, L. A., De Vis, J. B., de Bresser, J., Hendrikse, J., & Siero, J. C. W. (2020). Arterial CO2 pressure changes during hypercapnia are associated with changes in brain parenchymal volume. *European Radiology Experimental*, *4*(1), 1–7.

Vinje, V., Ringstad, G., Lindstrøm, E. K., Valnes, L. M., Rognes, M. E., Eide, P. K., & Mardal, K.-A. (2019). Respiratory influence on cerebrospinal fluid flow – a computational study based on long-term intracranial pressure measurements. *Scientific Reports*, *9*(1), 1–13.

Wang, Y., van Gelderen, P., de Zwart, J. A., Özbay, P. S., Mandelkow, H., Picchioni, D., & Duyn, J.

H. (2022). Cerebrovascular activity is a major factor in the cerebrospinal fluid flow dynamics. *NeuroImage*, 119362.

Wasserman, A. J., & Patterson, J. L., Jr. (1961). The cerebral vascular response to reduction in arterial carbon dioxide tension. *The Journal of Clinical Investigation*, *40*(7), 1297–1303.

Xu, F., Uh, J., Brier, M. R., Hart, J., Yezhuvath, U. S., Gu, H., Yang, Y., & Lu, H. (2011). The Influence of Carbon Dioxide on Brain Activity and Metabolism in Conscious Humans. *Journal of Cerebral Blood Flow and Metabolism: Official Journal of the International Society of Cerebral Blood Flow and Metabolism*, *31*(1), 58–67.

Xu, Z., Soh, Z., Kurota, Y., Kimura, Y., Hirano, H., Sasaoka, T., Yoshino, A., & Tsuji, T. (2024). Neuroimaging-based evidence for sympathetic correlation between brain activity and peripheral vasomotion during pain anticipation. *Scientific Reports*, *14*(1), 3383.

Yang, H.-C. S., Inglis, B., Talavage, T. M., Nair, V. V., Yao, J. F., Fitzgerald, B., Schwichtenberg, A. J., & Tong, Y. (2022). Coupling between cerebrovascular oscillations and CSF flow fluctuations during wakefulness: An fMRI study. *Journal of Cerebral Blood Flow and Metabolism: Official Journal of the International Society of Cerebral Blood Flow and Metabolism*, 271678X221074639.

Zhong, X., Polimeni, J. R., & Chen, J. J. (2024). Predicting the macrovascular contribution to resting-state fMRI functional connectivity at 3 Tesla: A model-informed approach. In *bioRxiv* (p. 2024.02.13.580143). https://doi.org/10.1101/2024.02.13.580143

Zhong, X. Z., & Chen, J. J. (2022). Resting-state functional magnetic resonance imaging signal variations in aging: The role of neural activity. *Human Brain Mapping*, *43*(9), 2880–2897.